

Biophysical Journal, Volume 97

Supporting Material

In vivo impedance of the gerbil cochlear partition at auditory frequencies

Wei Dong and Elizabeth S. Olson

Supplemental Material to Biophysical Journal “*In vivo* impedance of the gerbil cochlear partition at auditory frequencies” by Wei Dong and Elizabeth S. Olson

Abbreviations:

BF, best frequency; BM, basilar membrane; CAP, compound action potential; CP, cochlear partition; OC, organ of Corti; OHC, outer hair cell; P_{SV} , scala vestibule pressure; ΔP , pressure difference across the CP; RWM, round window membrane; SM, scala media; ST, scala tympani; SV, scala vestibuli; V_{BM} , basilar membrane velocity; Z , impedance of cochlear partition; Z_{real} , real part of Z ; $Z_{imaginary}$, imaginary part of Z .

1. Sources of phase uncertainty

The goal and strategy of these experiments was straightforward. However, a major challenge of the study was that it was not at all forgiving of small errors or uncertainty in phase. There are a number of sources of small phase uncertainty, and below we discuss them in turn. The specific motivation for the detailed exploration was the unexpected observation of a negative real part in the cochlear partition (CP) impedance. However, in the end we conclude that it is unlikely that any of the phase errors we document produced the observation.

1.1. Sensor calibration and phase offset

The sensors were calibrated by immersing them 1 mm beneath the surface of a vial of water that was attached to a vertical shaker with attached accelerometer (Bruel and Kjaer, type 4290). The vertical acceleration was set to produce a pressure of 0.2 Pa for a 1 mm immersion. The sensor sensitivity was measured from 200 Hz to 50 kHz. The sensitivity is typically flat with frequency to within ~ 2 dB through 40 kHz and often drops a few dB between 40 and 50 kHz (Fig 2 of (1)). Water calibration was performed after sensor construction and before and after experiments. The sensitivity can change due to very small disturbances of the sensitive membrane; this produces an uncertainty of $\pm \sim 10$ dB in the pressure measurements. The sensor output is expected to be in phase with pressure, and thus with the shaker acceleration and this phase relationship had been checked in the past. The results of the present study were very sensitive to phase so we took extra precautions to quantify phase offsets and variability and found that sensor output often lagged the pressure by a few degrees. In the frequency region from 4 to 20 kHz this value was $0^\circ - 14^\circ$, with an average of 7° . This wasn't a simple electronics delay, which would not vary from sensor to sensor. The variability was likely due to the sensor optical-mechanical coupling – the way the light was redirected back into the fiber after reflecting from the membrane.

The sensors are also calibrated in air, and the air calibration is usually similar to the water calibration. Then the sensor was positioned close to the membrane of a 1/4 inch Bruel & Kjaer microphone and ~ 2 -3 mm away from a Radio Shack speaker. The speaker was driven to produce pure tones with frequency from 0.2 to 60 kHz. Sensor sensitivity was found as the ratio of sensor voltage to the pressure as determined by the Bruel & Kjaer microphone. The sensor voltage phase was typically within a few degrees of the microphone voltage (Fig. 4 of (2)). An advantage of air calibrations is that they can easily be performed at both room and body temperature and thus provide a check of temperature sensitivity. Sensors were not used if the calibration shifted with temperature by more than 5 dB. The phase of sensor voltage relative to microphone voltage was stable with temperature.

In order to explore the effect of the phase offset, below we plot an invented impedance function that is a pure stiffness (Fig. S1). The imaginary and real parts are shown in the left panel, the magnitude and phase in the right panel. Next, we introduce a 7° lag in the impedance phase (such as would occur if the sensor output lagged the pressure by 7°) and a 14° lag, and see how these errors would affect the real and imaginary impedance values. The magnitude is kept fixed. The erroneous impedances are shown along with the original impedances, with thin (7°) and dashed (14°) lines. Where the impedance magnitude is large, the phase error introduced a relatively large change to the real part (which started out at zero). The imaginary part is reduced due to the phase errors, but because the imaginary part is large, the change is so small that it is not evident in the figure. Because the sign of the sensor phase error is negative, the error introduces a negative real part into the impedance and could produce an apparent negative resistance. However, if a sensor phase offset were responsible for the negative resistance, all measurements made with the same sensor would be expected to show it and that was not the case; see for example Fig. 2. This argues against the phase offset being responsible for the negative resistance.

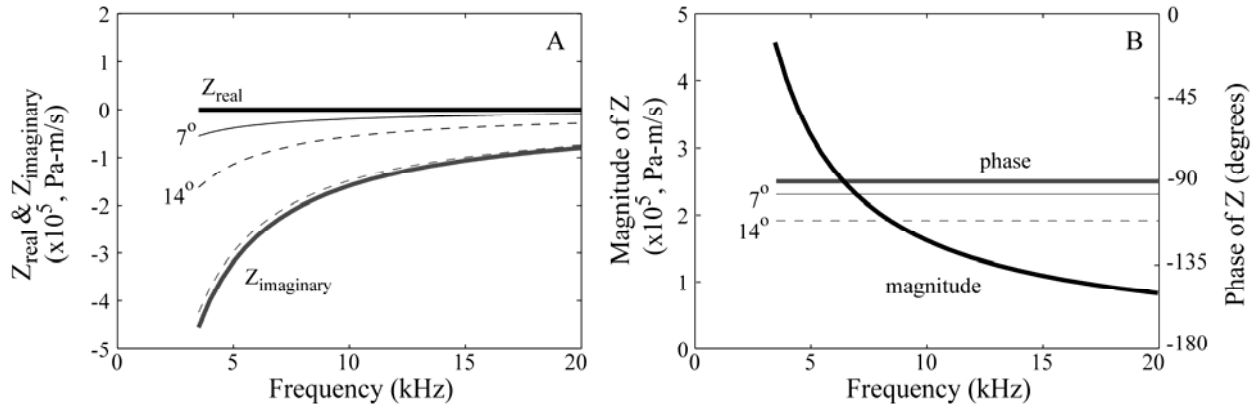


Fig. S1 Effect of sensor phase offset.

(A) Real and imaginary parts of Z . (B) Magnitude and phase of Z . Thicker, thin and dotted lines represent 0° (no error), 7° and 14° phase lags respectively.

1.2. Errors resulting from using P_{SV} to approximate ΔP

ΔP was found as P_{SV} (near the stapes) – 0 (zero), where the zero refers to atmospheric pressure in basal ST when the fluid is low in the RW. The RWM naturally lies very close to the BM in the base of the gerbil cochlea. After opening the bulla, the RWM sometimes bulges outward with perilymph, and at other times stays low. In the latter case there is only a very thin layer of fluid covering the BM. This was the desired condition, and when fluid welled up we wicked it out with a piece of tissue. P_{SV} near the stapes was used to approximate the pressure at the CP. This approximation only holds for frequencies well beneath the local BF, the well-sub-BF frequency region. Around the BF, the traveling wave wavelength is short, and close to the moving tissue of the CP fluid motion and pressure vary rapidly in space – this is the “short wave” region described in cochlear models. In particular, at frequencies near the BF, close to the BM the pressure goes through the same traveling wave delays as the BM motion, but even 100 μm from the BM, the pressure does not exhibit those delays and cannot be considered to be the local driving pressure needed for calculating Z (3, 4).

In contrast, at well-sub-BF frequencies, the pressure does not vary much with distance from the BM – this is the “long wave” region described in cochlear models. Judging from previous measurements of spatial pressure variations in the very base (1), P_{SV} measured distant from the CP can be used fairly well to find ΔP for frequencies $< \frac{1}{2}$ the local BF. This limited the study of Z here, with local BF ~ 40 kHz, to frequencies less than 20 kHz. Based on the earlier measurements the error introduced will be: approximately $\sim 12 - 20^\circ$ at a frequency half of the local BF, decreasing as frequency decreases ($\sim 7^\circ$ at $\frac{1}{4}$ BF), and increasing rapidly for higher frequencies. As the frequency begins to approach the BF, the V_{BM} phase shows cochlear traveling wave delay but P_{SV} measured distant from the BM does not. The predicted upward sweep of the phase error is apparent in our > 20 kHz results, and begins to be apparent even below 20 kHz. It is notable that this error makes the resistance appear more positive, so cannot be responsible for the observed negative resistance.

1.3. Optical contamination by the RWM

Even though the laser is focused on the BM, the RWM is in the optical path and light will be reflected from it. (The thin membrane is nearly transparent and the characteristics of the reflection would be similar from the air/fluid interface if the membrane itself were removed.) In order to estimate the effect of the RWM, we focused on it, and measured its response. The phase difference $P_{SV} - V_{RWM}$ is shown in Fig. S2 and discussed below.

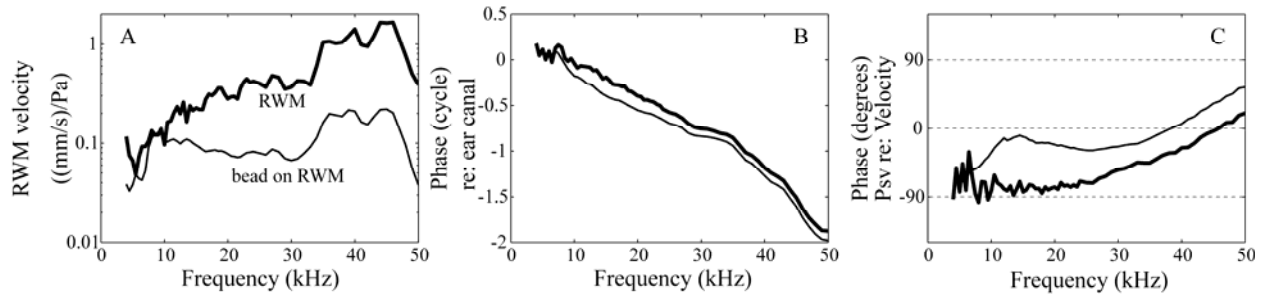


Fig. S2 Motion of RWM.

(A) RWM velocity with and without bead. (B) Phase referenced to ear canal pressure phase. (C) Phase of P_{SV} relative to V_{RWM} . (wg124, SPL = 80 dB)

Fig. S2 shows two measurements of RWM velocity, one directly from the RWM, the other from a gold-coated glass bead that is together with several beads on the RWM. When the RW fluid layer was thin the RWM motion (bold line) was similar to BM motion. On the other hand, the cluster of beads (thin line) diminished the amplitude of the RWM velocity and changed its phase (Fig. S2, A and B). We related the RWM velocity phase to the simultaneously measured P_{SV} in panel C. To facilitate comparison with Z results, the phase is plotted as P_{SV} phase re: RWM velocity phase. Without the beads the phase was close to -90° , similar to our results from the BM, confirming that the RWM moved with the BM when close to it. With the beads, the phase was closer to 0° . This suggests that the with-bead RWM motion more closely followed stapes motion, as a phase of 0° is as expected given the approximately resistive cochlear input impedance (5).

During our experiments the laser was focused on the BM and most of the signal will come from it; light from the RWM will also contribute, but will be attenuated by the optical sectioning afforded by the objective lens. de La Rochefoucauld et al. (6) discussed the signal

competition problem and showed that for motions somewhat less than the wavelength of the interferometer's HeNe laser (633 nm) the net response from the two signals could be like a weighted sum, with the weighting corresponding to the intensity of returning light. In the weighted sum picture, contaminating signal from the RWM would shift the apparent impedance phase positive, which would mask negative resistance, not contribute to it. However, the weighted sum picture turned out to be very sensitive to the optical path lengths between the two surfaces; with certain path lengths, the net response was not an average, but was outside the bounds of the individual signals, in both amplitude and phase. Therefore, although the RW motion by itself would lead to a positive resistance, the sum of the RW signal with the BM signal could produce phase variations in either the positive or negative direction. It is notable that path length variations of less than the wavelength of light produce different additive effects, so errors due to signal competition would be expected to produce a range of uncertainty, not a systematic shift. Therefore, while some amount of the variability we observe is likely due to signal competition, it is unlikely that signal competition produces the quite robust negative resistance apparent in our results.

1.4. Path length variation error

This is related to the above in that it also involves the effect of motion of the fluid above the BM. However, it is a different problem and we will see has a different effect. The path length variation error was described by Cooper and Rhode (7), when they discussed what they considered to be an anomalous BM displacement phase at low frequencies. These were frequencies at which the BM response amplitude was quite small – about the same size as the stapes motion. Since the cochlear fluid is nearly incompressible, the RWM motion is on average in phase with the stapes – when the stapes plunges in, the overall motion of the RWM is bulging out. (The true compressibility of the cochlear fluids will change this picture somewhat at very high frequencies.) The motion of the RWM will change the path length of the laser light through the fluid as it makes its way to the BM, and again as the reflected light makes its way back. Say the laser light passes from air (index of refraction $n_1=1$) through a saline layer ($n_2=1.3$) and then to the surface it is focused on (call it BM). The net change in the laser path length is what a laser interferometer system is actually measuring. Say the fluid surface moves with displacement d_1 and the BM moves with d_2 . If the two move exactly the same ($d_1=d_2$), the light reflected from d_2 would have a path length variation $2 \times n_1 d_2$ because there is no path length variation in the saline layer. (The factor two accounts for the round-trip.) This is the situation if the RWM is close to the BM and locally moves \sim with the BM, which seems to obtain in our measurements, based on Fig. S2. If the surface of the saline layer didn't move at all (e.g., if there were a cover slip) then $d_1=0$, the path length variation is all in the fluid, and the optical path length variation is $2 \times n_2 d_2$. In general the path length difference is $2 \times (n_1 d_1 + (d_2 - d_1) n_2)$, and when $n_1=1$ and $n_2=1.3$ this is $2 \times (1.3 d_2 - 0.3 d_1)$. It is instructive to figure the path length variation when the RWM moved as in the case with the beads in Fig. S2. There, the RWM (d_1) moved with a slight lead relative to the BM (d_2). However, the lead of d_1 enters in as a lag in the calculation $1.3 d_2 - 0.3 d_1$. This is different from the summed optical signals treated above in section 1.3; all of the light is considered to be reflected from the BM, but the moving RW surface still modifies the total variation in path length. In this case, the effect is systematic, with a velocity signal that would lag the actual velocity signal, and thus *could* lead to an apparent negative resistance.

1.5. Effect of cover slip on P_{SV} and V_{BM}

In order to satisfy the condition that $P_{ST} = 0$ in the base, the RW opening was left open, and the round window fluid was kept low. Unfortunately the fluid interface at the RWM could give rise to optical contamination or path length variation errors, as described above. Below we show the result of a measurement made with a glass cover slip on the RW, stabilizing the RW fluid. In Fig.S3 A–C V_{BM} is shown with and without the cover slip (solid and dotted lines respectively). In D–F the SV pressure is shown. The glass cover caused an increase in pressure of a few dB at all frequencies, and up to ~ 8 dB in the 20 – 40 kHz range. Thus, the presence of the cover on the RW modified cochlear mechanics. The phase changed little, but in the magnified view in F, the with-cover condition is seen to lead by $\sim 10^\circ$ in the ~ 7 to 10 kHz range. V_{BM} was generally a bit smaller with the cover slip, over a wide range of frequencies. The velocity phase also had a wide-frequency-band shift, and the with-cover condition lagged the without-cover condition by $\sim 30^\circ$. The combined pressure and velocity result, is that without the cover slip P_{SV} lagged V_{BM} by $\sim 90^\circ - 120^\circ$ and with the cover slip P_{SV} lagged V_{BM} by $\sim 55^\circ - 60^\circ$. The without-cover result suffers from the optical effects detailed above. The with-cover result suffers from the fact that we can no longer say $\Delta P \sim P_{SV}$. Now $\Delta P = P_{SV} - P_{ST}$, and P_{ST} is unknown. To understand P_{ST} , we need to ask what mechanical impedance the presence of the cover slip is likely to impart. The glass cover might impose some viscous resistance to the flow of fluid around it. This impedance would make the V_{BM} lag the pressure compared to the cover-less case without the added resistance, and this is the behavior observed in panel G. In our estimation the uncertainty in V_{BM} measurement due to the cover-less condition imposed less of a systematic problem than the uncertainty of ΔP in the covered condition.

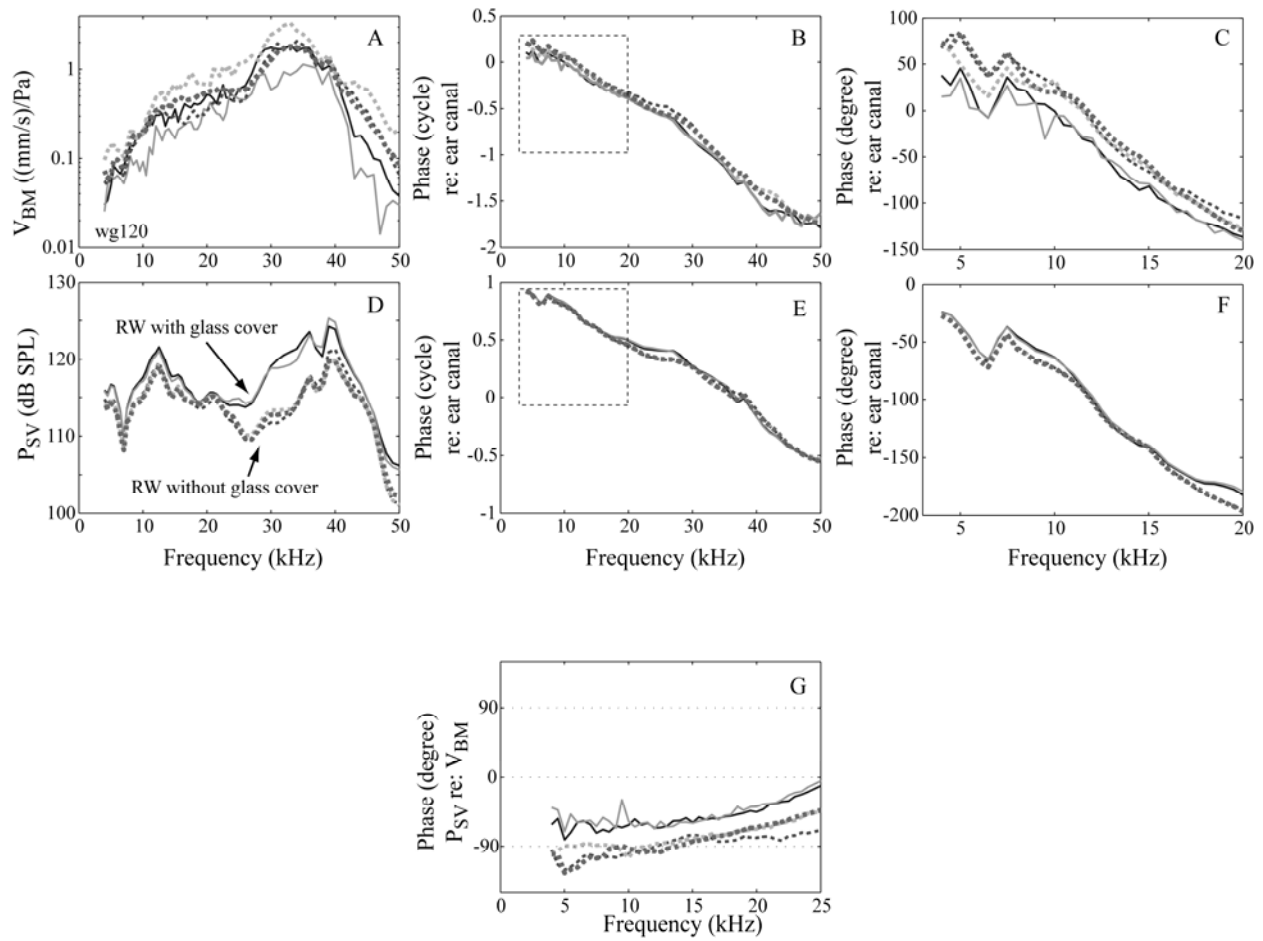


Fig. S3 Influence of the cover slip on the RW.

(A) V_{BM} . (B) Velocity phase referenced to ear canal pressure phase. (C) Enlarged velocity phase up to 20 kHz. (D) SV pressure. (E) Pressure phase referenced to ear canal pressure phase. (F) Enlarged velocity phase up to 20 kHz. (G) Phase difference between P_{SV} and V_{BM} . (Note P_{ST} is not known when the cover slip is in place.) Solid and dotted lines represent the condition with and without RW cover slip. (wg120, SPL = 90 dB)

2. Stability of P_{SV} and V_{BM} with different cochlear conditions

2.1. P_{SV} and its stability

P_{SV} near the stapes has been measured previously (e.g., (1, 8)) and the present results are consistent with those reports. In brief, P_{SV} at the stapes is typically quite flat with frequency up to 40 kHz, with a gain relative to the ear canal pressure of ~ 25 dB. The phase is delay-like, with a delay of ~ 30 μ s. There is often a notch in the amplitude and corresponding phase irregularity around 7 kHz. This has been noted in both P_{SV} and stapes motion and discussed previously (1, 8, 9). We have shown previously that insertion of the SV sensor does not perturb cochlear mechanics: the insertion can be done without changing ST pressure (3), CAP thresholds or distortion otoacoustic emissions (8, 10). P_{SV} near the stapes increases linearly with SPL even in active cochleae (3). P_{SV} is stable with stable cochlear condition, and here we pay particular attention to the effect of the RW fluid level. As described in the methods, the RW fluid was maintained quite low. Fig. S4 shows P_{SV} responses to single tone stimuli under several cochlear conditions. The amplitude and phase changed slightly with changes in fluid level at frequencies from 25 to 40 kHz. The changes were within 2 dB and 3° . Three hours post-mortem, the RW became relatively dry and the pressure changed more, especially at frequencies above 30 kHz, with variations in amplitude up to 5 dB and in phase of 4° to 10° . From 4 – 30 kHz the amplitude change was less than 3 dB and the phase change was less than 3° except for two wiggles to $\sim 4^\circ$. Even though there were variations in the amplitude and phase under these slightly different cochlear conditions, the maximum variation occurred in the high frequency region, where the changes might be related to changes in the influence of the cochlear traveling wave. This frequency region is not analyzed in the present study. From 4 to 20 kHz, the maximum variation was 3 dB in amplitude and $\sim 3^\circ$ in phase. Therefore, P_{SV} was adequately stable with time and condition.

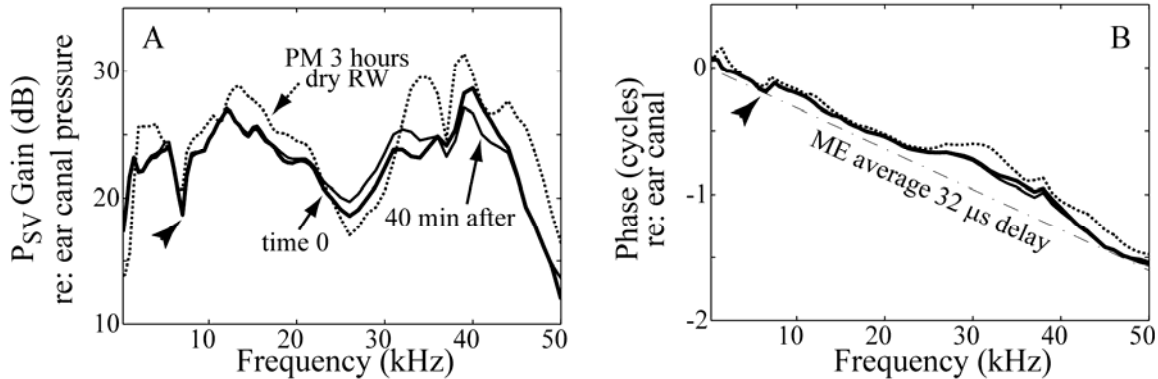


Fig. S4 Stability of P_{SV} .

(A) P_{SV} amplitude. (B) P_{SV} phase. Pressure responses were measured without a cover slip on the RW, with the standard RW fluid level at time 0 (thick line), with a thin layer of RW fluid (thinner line, 40 minutes later) and post-mortem about three hours with relatively dry RW (thin dotted line). At frequencies below 20 kHz, the amplitude and phase variations were small. Amplitude of P_{SV} was normalized to ear canal pressure and phase of P_{SV} was referenced to ear canal pressure. (wg120).

2.2. V_{BM} and its stability at well-sub-BF frequencies

As noted and documented above, it is possible to insert the SV pressure sensor without changing cochlear responses. However, usually the responses of the very basal region are linearized by the insertion. (Even in intact cochleae, measurements of the BM velocity in the very basal region usually show linear scaling with SPL (exceptions in (11)). This region is quite

exposed, which might contribute to its fragility.) We have maintained that the absence of nonlinearity in the region under study does not diminish our results at frequencies well-sub-BF, and Fig. S5 supports this statement. It shows CAP and V_{BM} responses before (solid lines) and after (dotted lines) inserting the SV sensor. With the cochlea intact, the CAP responses were typical, with thresholds ~ 20 dB up to 22 kHz and higher at higher frequencies. V_{BM} measured at stimulus levels of 70, 80 and 90 dB SPL are plotted normalized to the stimulus level in Fig. S5 B. Before insertion, at frequencies above ~ 25 kHz the responses were nonlinear: normalized responses were larger at the lower stimulus level, indicating that the cochlear amplifier was functioning. At 70 dB the BF was 36 kHz and this shifted to slightly lower frequencies at the higher stimulus levels. Up to ~ 30 kHz the phase (Fig. S5 C) was quite similar to that of P_{SV} (Fig. S4 B), but accumulated more delay in the BF region due to the cochlear traveling wave in the velocity, which is not apparent in the pressure far from the OC (3).

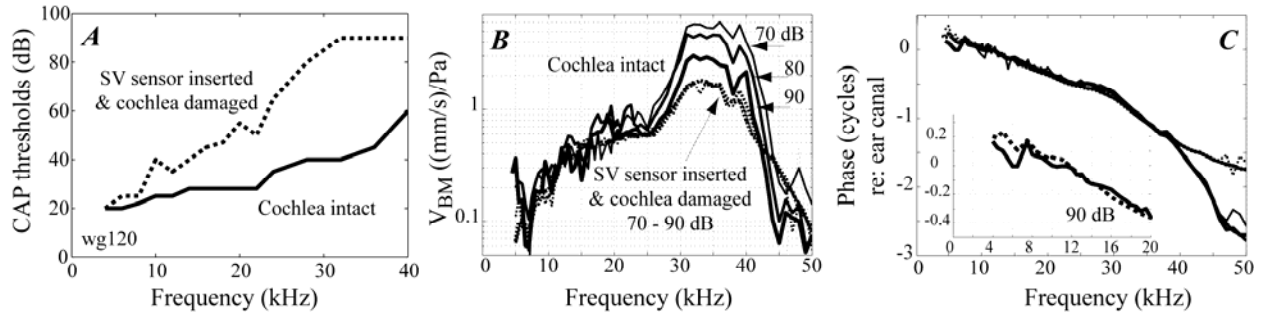


Fig. S5 Stability of V_{BM} under different cochlear conditions.

(A) CAP thresholds under cochlea intact and damaged (with SV sensor inserted) conditions. Solid and dotted lines identify the intact and damaged condition in all panels. (B) Normalized V_{BM} amplitude, stimulus level 70 to 90 dB SPL. Compressive nonlinearity was initially apparent but the responses became linear after the SV sensor was inserted. (C) V_{BM} phase. The small panel enlarges the view of the phases up to 20 kHz; 90 dB SPL responses shown. (The RWM was intact and the RW opening was covered by a glass cover slip to control the fluid level. A cover slip was used in order to study changes independent of potential RW fluid changes.) (wg120).

After inserting the sensor, the CAP thresholds increased in a frequency dependent manner. (These changes were relatively severe and in other cases were restricted to the highest frequencies.) V_{BM} amplitude, measured at approximately the same location as before inserting the sensor, was reduced in the BF region and became linear (normalized responses overly). Below 25 kHz there was little change in the amplitude. The phase flattened out above ~ 40 kHz, likely due to fast-wave predominance (1). Below 40 kHz there was little change in the phase. Because even small phase changes are important in this study, in the inset the 4 – 20 kHz region is expanded, with only 90 dB results shown for clarity. Here we can see that from 7 – 20 kHz, the phase showed no significant change post-damage. However, there is a ~ 0.1 cycle (36 degree) shift in the phase 6 kHz and below. This shift is very similar to the phase variation at slightly different locations in Fig. 2, and thus cannot be clearly attributed to the damaged condition. Overall, Fig. S5 confirms the robustness and stability of the v_{BM} responses in the well-sub-BF region and indicates that the well-sub-BF results in the paper are applicable to the healthy cochlea.

3. Cochlear model of influence of negative resistance

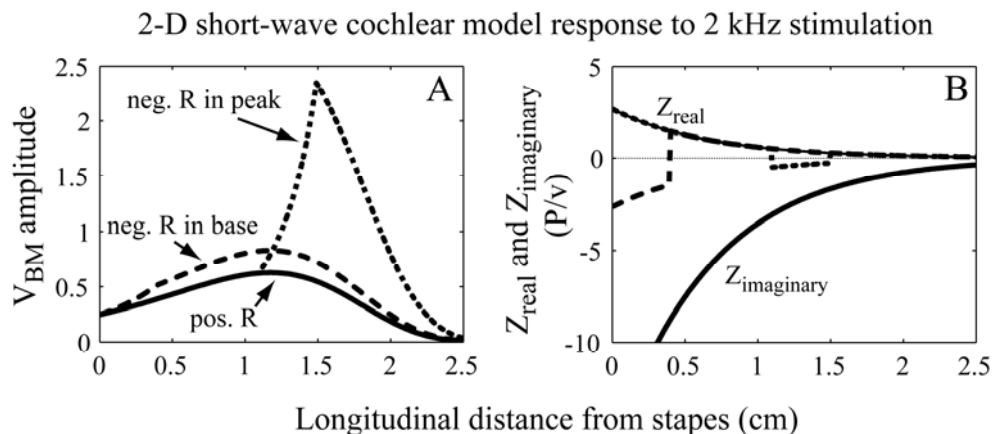


Fig. S6 2-D short-wave cochlear model used to probe the model response with negative resistance applied in the very base and in the peak region.

(A) V_{BM} amplitude; (B) Real and imaginary parts of Z .

Figure S6 shows a model derived from the human cochlear model developed by Siebert (12). (It has not been modified for gerbil as that was not necessary to make the point.) The real part of Z was assigned an absolute value 1/6 of the imaginary part in both modified (dashed lines) and unmodified (solid lines) cases. Z_{real} was made negative over a 4 mm region either in the base, or close to the passive peak (dashed lines in B). The model response is much more sensitive to negative resistance when it is applied in the peak region (A, lines with short dashes) than in the basal region (A, lines with larger dashes).

4. Extensions to other species

Ruggero et al. (13) estimated basal CP stiffness in several species based on combining P_{SV} and V_{BM} measurements made by different groups in different individual animals. Those estimates, along with others from direct stiffness measurements were tabulated in their table IV, with the following average results: cat, $S \sim 3.4 \times 10^9$ Pa/m; guinea pig, $S \sim 1.5 \times 10^9$ Pa/m; chinchilla, $S \sim 0.4 \times 10^9$ Pa/m. These values are within the entire range reported for gerbil base in Fig. 6. The values for cat are closest to the stiffness values of the present report and to the cluster of values in Fig. 6.

An advance of the present study was that the simultaneous measurement of pressure and motion allowed for a more precise measure of impedance, which included phase. We found that at well-sub-BF frequencies the phase of Z was close to -90° ; thus the CP impedance was stiffness-dominated. Below we use previously published results to estimate impedance phase from other species. We start with the Z phase definition: $\phi_Z = \phi_{\Delta P} - \phi_{V_{BM}} \approx \phi_{P_{SV}} - \phi_{V_{BM}}$. The approximate equality holds for $P_{ST} \approx 0$ and with V_{BM} measured near the RW. In the comparisons to other species below, BM measurements were not made under conditions of low RW fluid but were all made through the RW opening. Thus, the comparison is not perfect but is still meaningful. Carrying on,

$\phi_Z \approx (\phi_{P_{SV}} - \phi_{V_{STAPES}}) - (\phi_{V_{BM}} - \phi_{V_{STAPES}}) \approx \phi_{Z_{COCHLEA}} - (\phi_{V_{BM}} - \phi_{V_{STAPES}})$. Here the phase is in two parts; $\phi_{Z_{COCHLEA}} = (\phi_{P_{SV}} - \phi_{V_{STAPES}})$ is the cochlear input impedance and $\phi_{V_{BM}} - \phi_{V_{STAPES}}$ is

the phase of V_{BM} relative to the stapes velocity. The cochlear input impedance has been measured in several species (5, 14-18) and through a wide frequency range it was predominantly resistive (phase close to zero), confirming that energy delivered at the stapes is absorbed by the cochlea. Assuming $\phi_{ZCOCHLEA} = 0$, $\phi_Z \approx -(\phi_{VBM} - \phi_{VSTAPES})$. The relationship $\phi_{VBM} - \phi_{VSTAPES}$ is available from much of the BM motion literature, in which it is common to reference BM motion to stapes motion. If ϕ_Z is -90° (CP impedance stiffness dominated) then $\phi_{VBM} - \phi_{VSTAPES}$ at well-sub-BF frequencies will be $+90^\circ$. Figure S7 shows the phase of BM motion relative to stapes in several species. (The phase of chinchilla from (19) was referenced to umbo motion imaged from inside the bulla; under the assumption that stapes and umbo move together the phase was offset by a half cycle here.) At frequencies an octave below the BF the phases varied slowly with frequency and were generally close to $+90^\circ$. (chinchilla = CH, (19, 20), gerbil = GB, (11, 21)) and guinea pig = GP, (7)). Therefore, the phases of CP impedance were generally close to -90° for these animals, representing a stiffness-dominated impedance.

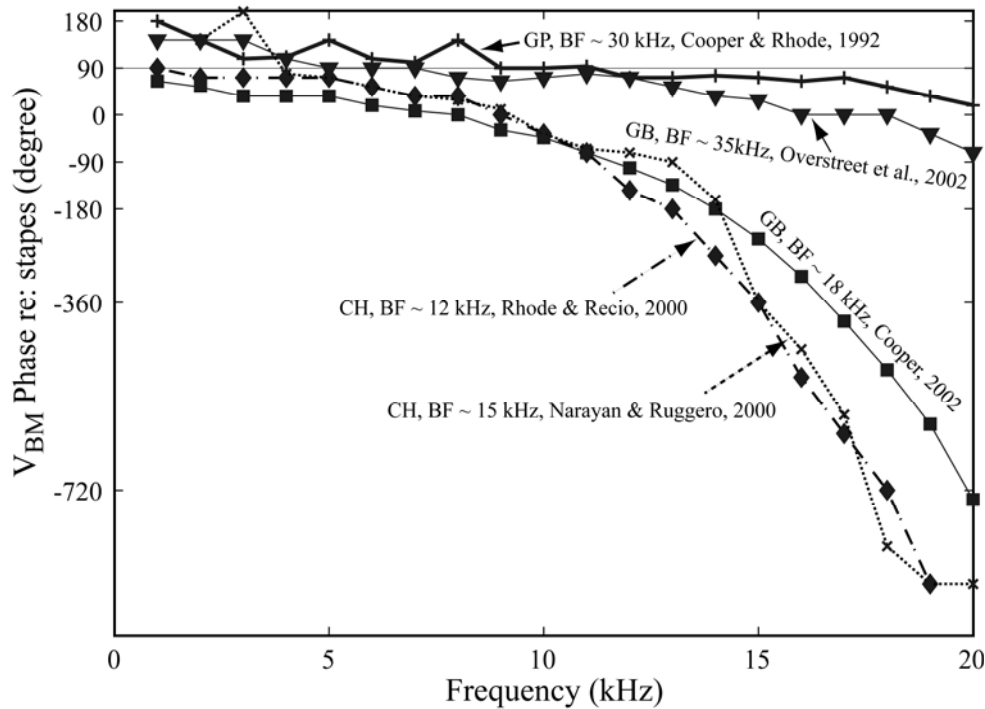


Fig. S7 The BM phase relative to inward stapes motion in several species: guinea pig (GP), gerbil (GB) and chinchilla (CH).

References

1. Olson, E. S. 1998. Observing middle and inner ear mechanics with novel intracochlear pressure sensors. *J Acoust Soc Am* 103:3445-3463.
2. Ravicz, M. E., E. S. Olson, and J. J. Rosowski. 2007. Sound pressure distribution and power flow within the gerbil ear canal from 100 Hz to 80 kHz. *J Acoust Soc Am* 122:2154-2173.
3. Olson, E. S. 2001. Intracochlear pressure measurements related to cochlear tuning. *J Acoust Soc Am* 110:349-367.

4. Olson, E. S. 1999. Direct measurement of intra-cochlear pressure waves. *Nature* 402:526-529.
5. de la Rochefoucauld, O., W. F. Decraemer, S. M. Khanna, and E. S. Olson. 2008. Simultaneous measurements of ossicular velocity and intracochlear pressure leading to the cochlear input impedance in gerbil. *J Assoc Res Otolaryngol* 9:161-177.
6. de La Rochefoucauld, O., S. M. Khanna, and E. S. Olson. 2005. Recording depth and signal competition in heterodyne interferometry. *J Acoust Soc Am* 117:1267-1284.
7. Cooper, N. P., and W. S. Rhode. 1992. Basilar membrane mechanics in the hook region of cat and guinea-pig cochleae: sharp tuning and nonlinearity in the absence of baseline position shifts. *Hear Res* 63:163-190.
8. Dong, W., and E. S. Olson. 2006. Middle ear forward and reverse transmission in gerbil. *J Neurophysiol* 95:2951-2961.
9. Ravicz, M. E., N. P. Cooper, and J. J. Rosowski. 2008. Gerbil middle-ear sound transmission from 100 Hz to 60 kHz. *J Acoust Soc Am* 124:363-380.
10. Dong, W., and E. S. Olson. 2008. Supporting evidence for reverse cochlear traveling waves. *J Acoust Soc Am* 123:222-240.
11. Overstreet, E. H., 3rd, A. N. Temchin, and M. A. Ruggero. 2002. Basilar membrane vibrations near the round window of the gerbil cochlea. *J Assoc Res Otolaryngol* 3:351-361.
12. Siebert, W. M. 1974. Ranke revisited--a simple short-wave cochlear model. *J Acoust Soc Am* 56:594-600.
13. Ruggero, M. A., N. C. Rich, L. Robles, and B. G. Shivapuja. 1990. Middle-ear response in the chinchilla and its relationship to mechanics at the base of the cochlea. *J Acoust Soc Am* 87:1612-1629.
14. Lynch, T. J., 3rd, W. T. Peake, and J. J. Rosowski. 1994. Measurements of the acoustic input impedance of cat ears: 10 Hz to 20 kHz. *J Acoust Soc Am* 96:2184-2209.
15. Slama, M., M. Ravicz, H. Nakajima, W. Dong, and J. J. Rosowski. 2008. Measurements of Middle-Ear Pressure Gain and Cochlear Input Impedance in the Chinchilla In 31rd the Association for Research in Otolaryngology MidWinter Meeting, Phoenix, AZ.
16. Aibara, R., J. T. Welsh, S. Puria, and R. L. Goode. 2001. Human middle-ear sound transfer function and cochlear input impedance. *Hear Res* 152:100-109.
17. Nakajima, H. H., W. Dong, E. S. Olson, S. N. Merchant, M. E. Ravicz, and J. J. Rosowski. 2009. Differential intracochlear sound pressure measurements in normal human temporal bones. *J Assoc Res Otolaryngol* 10:23-36.
18. Dallos, P. 1970. Low-frequency auditory characteristics: Species dependence. *J Acoust Soc Am* 48:489-499.
19. Rhode, W. S., and A. Recio. 2000. Study of mechanical motions in the basal region of the chinchilla cochlea. *J Acoust Soc Am* 107:3317-3332.
20. Narayan, S. S., and M. A. Ruggero. 2000. Basilar-membrane mechanics at the hook region of the chinchilla cochlea. In *Recent Developments in Auditory Mechanics*. H. Wada, T. Takasaka, I. K., K. Ohyama, and T. Koike, editors. World Scientific, Singapore. 95 - 101.
21. Cooper, N. P. 2002. Basilar membrane vibrations in the basal turn of the gerbil cochlea. In 23th the Association for Research in Otolaryngology MidWinter Meeting, St. Petersburg Beach, Florida, USA.